EDGE ARTICLE

Check for updates

A singlet oxygen self-reporting photosensitizer for cancer phototherapy†

Tao Xiong,[a] Mingle Li,[c] Yingchao Chen,[a] Jianjun Du, [ID] [ab] Jiangli Fan [ID] [ab] and Xiaojun Peng [ID] *[ab]

Photodynamic cancer therapy has attracted great attention with the increasing threat of tumors, and improving its therapeutic efficacy is highly desirable. However, due to the highly efficient intersystem crossing potency to generate singlet oxygen ($^1O_2$), high-efficiency photosensitizers often suffer from weak fluorescence and excess injury to normal tissue. To overcome these obstacles, here we show a reliable self-reporting strategy for real-time monitoring of therapeutic progression. As a proof of concept, a molecular dyad is designed by connecting benzo[*a*]phenoselenazinium (**NBSe**) to rhodamine (**Rh**), namely **Rh-NBSe**, where the fluorescence of the **Rh** unit is initially suppressed by the fluorescence resonance energy transfer mechanism, but enabled to recover as feedback signal once the reaction with photosensitized $^1O_2$ takes place. The observed fluorescence increases by irradiation *in vitro* and *in vivo* successfully reflect the real-time $^1O_2$ generation speed in photodynamic therapy. In addition, the favorable therapeutic advantages of **Rh-NBSe** are also verified, for example, the high Φ_Δ (0.8) and the low IC$_{50}$ (0.2 μM, 6 J cm^{-2}). Based on the therapeutic ability and real-time $^1O_2$ self-reporting ability, **Rh-NBSe** demonstrates significant potential for self-regulating phototherapy.

Introduction

Cancer is currently one of the most lethal diseases in global healthcare, and it has been estimated that 18.1 million new cancer cases were diagnosed and 9.6 million cancer deaths occurred worldwide in 2018.[1,2] With the development of clinical treatment, photodynamic therapy (PDT) has drawn more and more attention due to the unique advantages of non-invasiveness, spatiotemporal accuracy and synergism.[3–7] The photosensitizers (PSs), as crucial elements, can transfer the endogenous oxygen to reactive oxygen species (ROS) for therapy.[8–12] In particular, benzo[*a*]phenoselenazinium (**NBSe**) has potential for efficient cancer phototherapy, thanks to its ultrahigh singlet oxygen quantum yield (Φ_Δ) in light and non-toxicity in the dark.[13,14] However, the negligible fluorescence quantum yield (0.03) of **NBSe** has limited its use in PDT.[13] Meanwhile, excessive light irradiation or PS dosages often lead to the risks of damage to normal tissue in PDT.[15] To address these problems, self-reporting PSs can be a good choice, which report the feedback signals to visualize some elements (*e.g.* singlet oxygen ($^1O_2$), superoxide radical, and apoptosis) for

diagnosis and control.[11,16–19] Based on a self-reporting strategy, **NBSe** has the potential to realize visualization in PDT and offer feedback to the treatment process. As a vital therapeutic weapon, the $^1O_2$ produced by PSs in light can destroy proteins or organelles in tumor cells.[20] There is no doubt that the generation of $^1O_2$ *in situ* can affect the therapeutic intensity during irradiation.[21] Therefore, the imaging and tracing of $^1O_2$ are meaningful to monitor therapeutic processes and decrease the risk of damage to normal tissues. However, the short lifetime (∼40 ns) and limited spread distance (∼20 nm) result in the difficulty of real-time imaging of $^1O_2$ during phototherapy, especially for targeted tumor tissues.[22]

To date, structures such as vinyl dithioether, aminoacrylates, and disulfanyl–ethyl carbonate have been found to have special response to ROS.[17,23] Of which, vinyl dithioether can realize efficient $^1O_2$ response by [2 + 2] cycloaddition reactions, and has better biological stability *in vivo*.[24] Usually, self-reporting PSs are combined with two or more segments, realizing therapy and affording fluorescent feedback after the reaction with linker. Some strategies, such as fluorescence resonance energy transfer (FRET), intramolecular charge transfer and electronic energy transfer, can be good choices to realize fluorescence reporting in PDT.[25–27] Using these $^1O_2$ active structures as linker, the fluorescence can be gradually released as feedback to control the phototherapy process during the irradiation period. Unfortunately, self-reporting PSs have not been much researched in the past; instead, these $^1O_2$ sensitive linkers are more commonly used for prodrug release.[28,29] Moreover,

[a] State Key Laboratory of Fine Chemicals, Dalian University of Technology, Dalian 116024, China. E-mail: pengxj@dlut.edu.cn

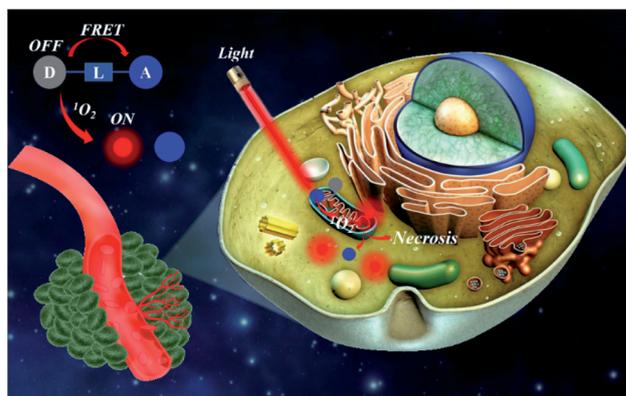*[b] Shenzhen Research Institute, Dalian University of Technology, Shenzhen 518057, China*

[c] Department of Chemistry, Korea University, Seoul 02481, Korea

focusing on the fluorescence reporting potency, the therapeutic efficacy of self-reporting PSs is always ignored. Thus, to develop $^1O_2$ self-reporting PSs for high-efficiency therapy is still meaningful.

Herein, we designed a new $^1O_2$ self-reporting PS based on the **NBSe** structure, which is expected to have both real-time fluorescence reporting ability and favorable therapeutic ability. With rhodamine (**Rh**) moiety as donor and **NBSe** moiety as acceptor, a FRET-based PS was constructed after connection *via* (*Z*)-1,2-bis(alkylthio)ethene (vinyl dithioether structure), named **Rh-NBSe** (Fig. 1a). As control, a molecule without the vinyl dithioether linker (direct click reaction) was also designed in the work, named **Rh-NBSe-1** (Fig. 1b). In **Rh-NBSe**, the fluorescence of donor (**Rh**) can be initially quenched due to the FRET process (Scheme 1),[17,30] while the linker would be cleaved upon irradiation, resulting in the release of fluorescence as feedback. Using **Rh** as donor, the high fluorescence quantum yield can provide stronger fluorescent differentiation reporting and overcome the imaging problem of **NBSe**.[31,32] Both for **Rh-NBSe** and **Rh-NBSe-1**, the double-cationic donor–acceptor (D–A) structure has advantages of good solubility and dispersibility, which can efficiently decrease the self-aggregation in aqueous solution. Moreover, cationic PSs are more likely to accumulate in tumor sites because of the lower negative membrane potential of tumors, and the structure inherent targeting (SIT) ability has been identified in some cationic molecules, including **Rh** and **NBSe**.[33,34] Therefore, the FRET-based PS with SIT ability and double cationic D–A structure has the potential to realize

Scheme 1 Sketch of therapy and fluorescence reporting of **Rh-NBSe**.

simultaneously integrated imaging, efficient therapy, and real-time $^1O_2$ reporting both *in vivo* and *in vitro*.

Results and discussion

Spectral properties

As a proof of concept, both **Rh-NBSe** and **Rh-NBSe-1** were synthesized using the routes shown in Scheme S1,† and the intermediates and products were characterized (Fig. S13–S30†) by mass spectra and nuclear magnetic resonance. To study the D–A structure in **Rh-NBSe** or **Rh-NBSe-1**, UV-visible absorption spectra were used to identify the components. As shown in
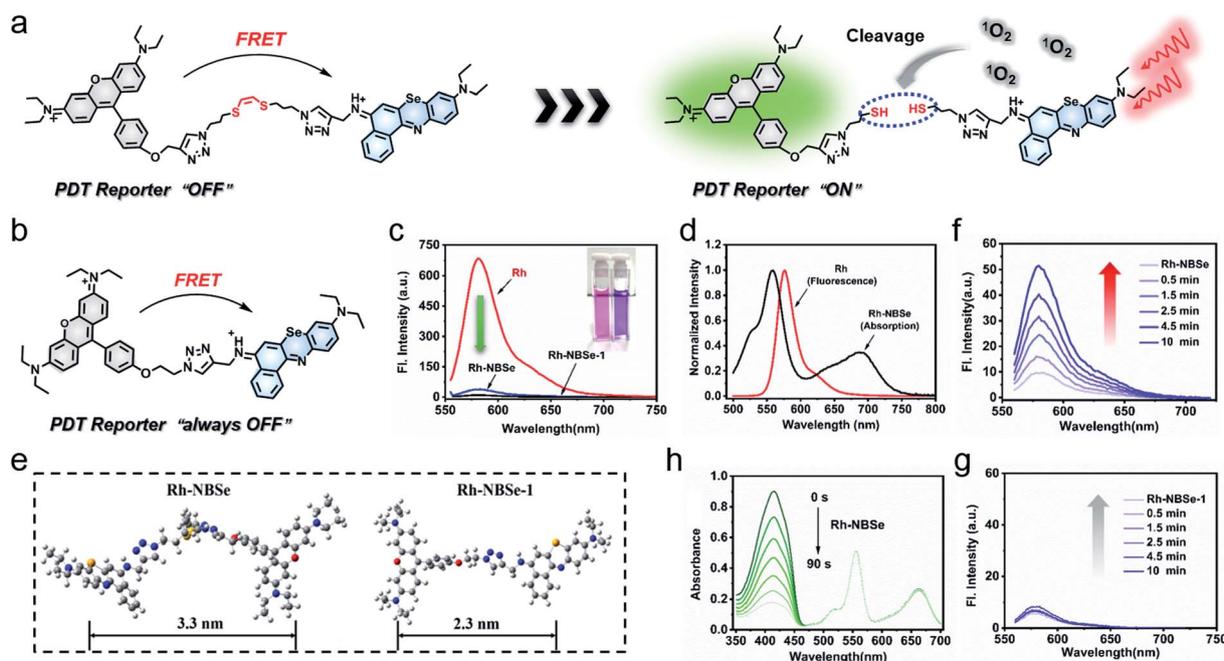

Fig. 1 Schematic illustrations of (a) **Rh-NBSe** and (b) **Rh-NBSe-1**. (c) Fluorescence emission comparison of **Rh-NBSe**, **Rh-NBSe-1** and **Rh** in PBS of 6 μM. (d) Spectral overlap between **Rh** emission and **Rh-NBSe** absorption in aqueous solution. (e) Molecular distance between **Rh** and **NBSe** moieties of **Rh-NBSe** or **Rh-NBSe-1**. Fluorescence recovery of (f) **Rh-NBSe** and (g) **Rh-NBSe-1** after irradiation for different times. (h) Singlet oxygen quantum evaluation of **Rh-NBSe** using 1,3-diphenylisobenzofuran (DPBF) as scavenger. The decay spectra were recorded at an interval of 15 s irradiation (3 mW cm^{-2}).

Fig. S1,† the spectra of **Rh-NBSe** and **Rh-NBSe-1** are both consistent with the overlap of **Rh** and **NBSe** in DCM, and show little spectral difference in water. The spectral results verify the combined D–A construction, and express the independence of absorption of donor/acceptor. Though **Rh** and **Rh-NBSe** both show lower absorption and molar extinction coefficient (ε) of maximum absorption in water compared with **Rh** in DCM (Fig. S2†), **Rh-NBSe** can still retain 76% maximum absorption, suggesting the sustaining of solubility after the combination with **NBSe**. Moreover, the step-up absorption spectra (6–36 μM, at intervals of 6 μM) showed good linearity at maximum absorption peak ($R = 0.9999$), representing favorable dispersing performance in aqueous solution.

By connection with **NBSe**, both **Rh-NBSe** and **Rh-NBSe-1** showed weak fluorescence compared with **Rh** at the same concentration in aqueous solution (Fig. 1c), in which the fluorescence intensity dropped to 36.77 and 9.71 (that of **Rh** was 684 a.u.), respectively. The results verified the fluorescence quenching, because of the FRET between **Rh** and **NBSe** moieties. From the normalized intensity shown in Fig. 1d, the fluorescence spectrum of **Rh** and the absorption spectrum of **NBSe** exhibit obvious spectral overlap at 580–650 nm, which is a prerequisite for FRET. Also, FRET needs a suitable molecular distance (1–10 nm) to transfer energy; the distances between **Rh** and **NBSe** moieties of **Rh-NBSe**/**Rh-NBSe-1** were calculated to be 3.3/2.3 nm using Gauss software, respectively (Fig. 1e). Both the spectral overlap and molecular distance meet the demands of FRET, and thus **Rh-NBSe** can realize fluorescence reporting by the breakage of linker due to the off state of FRET.

Under irradiation, the **Rh** fluorescence of **Rh-NBSe** will recover when the linker is cut by $^1O_2$, leading to the separation of donor and acceptor. Here we tested the fluorescence spectra of **Rh-NBSe** in PBS when irradiated by 660 nm LED light (20 mW cm^{-2}), and the fluorescence increase was recorded after a series of irradiation times (0.5, 1.5, 2.5, 4.5, 10 min). As shown in Fig. 1f, the maximum fluorescence increase was from 9.7 to 51.1 a.u. after 10 min irradiation (5.3-fold). By contrast, **Rh-NBSe-1** exhibits negligible signal changes after irradiation (Fig. 1g), demonstrating the property of (Z)-1,2-bis(alkylthio)ethene. These results revealed the self-reporting ability of **Rh-NBSe**, which showed a correlation between fluorescence and irradiation time. Indeed, the fluorescence change can reflect the real-time $^1O_2$, expecting to feedback therapy according the visual signals.

PDT efficacy evaluation in cells

Since the $^1O_2$ generation ability of PSs generally determines the therapeutic efficacy in PDT,[35] we calculated the Φ_Δ of the molecules. As shown in Fig. 1h, DPBF ($^1O_2$ scavenger) absorption spectra show rapid decay at an interval of 15 s irradiation when added to **Rh-NBSe**. And the control molecule **Rh-NBSe-1** or **Rh** + **NBSe** (two molecules at the same concentration) shows similar linear decay (Fig. S3†). Using methyl blue (**MB**) as reference ($\Phi_\Delta = 0.57$), the Φ_Δ of **Rh-NBSe**, **Rh-NBSe-1** and **Rh** + **NBSe** were estimated to be 0.8 by a reference method shown in ESI.† These results revealed the similar Φ_Δ value for these three

groups, suggesting the consistent $^1O_2$ generation ability of **NBSe** moiety with/without linker. Besides, to confirm the generation of $^1O_2$ in cells, 2,7-dichlorodihydrofluorescein diacetate (DCFH-DA) was selected, which can hydrolyze to DCFH in cells and then ROS oxide DCFH to DCF with bright green fluorescence.[36] As shown in Fig. S4,† only the group of PDT shows bright green fluorescence, suggesting the potent intracellular ROS generation ability of **Rh-NBSe** and **Rh-NBSe-1**.

Furthermore, to directly evaluate the therapeutic efficacy of **Rh-NBSe** *in vitro*, live/dead cell imaging in 4T1 cells was conducted using a calcein-AM/PI kit, whereby calcein-AM can be hydrolyzed into calcein and emit green fluorescence in living cells and PI can selectively embed into DNA double helix in dead cells to give red fluorescence.[22] As shown in Fig. 2a, **Rh-NBSe** exhibits almost all green fluorescence, meaning satisfactory biosafety in the dark. In contrast, strong red fluorescence of PI occurs in the group of PDT, which shows strong phototoxicity. Besides, we also tested the cell viability of different concentrations of **Rh-NBSe** in dark/light using MTT assays.[37] Under different exposure times (0, 5, 10 min), the cell viability was measured (Fig. 2b), which revealed the obvious phototoxicity. And the slight difference of cell viability between 5/10 min groups suggested the low light dose demand. Meanwhile, the phototoxicity *in vitro* was also compared with that of Chlorin e6 (**Ce6**), as shown in Fig. 2c; both **Rh-NBSe** and **Ce6** keep >90% viability in the dark, but dramatically decreased in light, especially for **Rh-NBSe**. The IC$_{50}$ of **Rh-NBSe** was calculated to be 0.2 μM, while that of Ce6 was 1.1 μM at the same conditions.
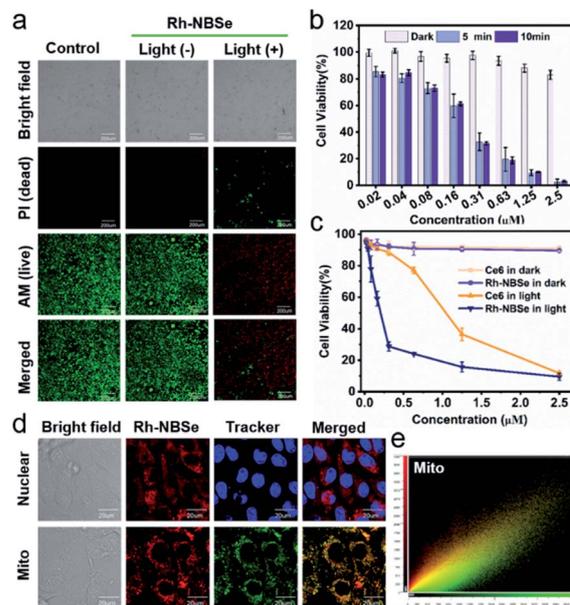

Fig. 2 (a) Live/dead cell imaging using calcein-AM/PI kit after 5 min irradiation (20 mW cm^{-2}). Ex: 488 nm, Em: 505–545 nm (calcein-AM); Em: 620–700 nm (PI). (b) MTT assays of **Rh-NBSe** with 0, 5 and 10 min irradiation (20 mW cm^{-2}). (c) Cell viability comparison of Ce6 and **Rh-NBSe** both in dark and light (5 min). (d) Mitochondria colocalization imaging. (e) Colocalization analysis of Mito using CLSM. Data are shown as mean ± SD ($n = 6$).

Subcellular localization and therapeutic mechanism

Subcellular organelle localization generally decides the mechanism of cell death, and influences the therapeutic efficacy. To identify the actual localization, colocalization assays were conducted using commercial dyes. **Rh-NBSe** showed better mitochondria (Mito) colocalization (Fig. 2d) and good localization ratio with Mito Tracker Green (Fig. 2e). Meanwhile, the Pearson coefficient in Mito was calculated to be 0.896; as a comparison, that of lysosome was 0.473 and nucleus was 0. To further analyze the therapeutic process, we labelled the cellular membrane with DiO (membrane dye), and used PI to indicate

the cell viability.[38] As shown in Fig. S5,† obvious cell death but intact membrane were observed after 30 min post-irradiation. Then the cellular membrane starts to break after 50 min, and is almost completely broken at 1 h. Taken together, we suspected that the mitochondria could be quickly destroyed after phototherapy, resulting in cellular necrosis, but not apoptosis. By Annexin V-FITC/PI kit staining, in which FITC-labelled recombinant human Annexin V particularly binds to phosphatidylserine of outer surface of apoptotic cells,[39] the PDT group showed red fluorescence in cellular nucleus and negligible green fluorescence (Fig. S6†), demonstrating the necrosis mechanism in PDT for **Rh-NBSe**. In addition, the group with PDT and NaN_3 (10 mM, $^1O_2$ scavenger) showed negligible fluorescence both for FITC and PI, indicating the ROS.
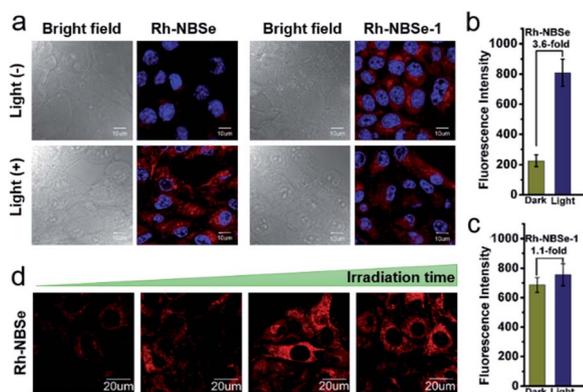

Fig. 3 (a) Fluorescence reporting of **Rh-NBSe** and **Rh-NBSe-1** in 4T1 cells before and after irradiation (660 nm, 20 mW cm^{-2} × 5 min). Quantitative fluorescence comparison before and after 5 min irradiation of (b) **Rh-NBSe** and (c) **Rh-NBSe-1** calculated by CLSM. (d) Fluorescence increase of **Rh-NBSe** at different times post-irradiation.

Fluorescence reporting in cells and *in vivo*

Aiming to demonstrate the fluorescence recovery in bio-system followed by the PDT process, the fluorescence variations of **Rh-NBSe** and **Rh-NBSe-1** were compared before/after irradiation using Hoechst 33342 as indicator. As shown in Fig. 3a, **Rh-NBSe** exhibits obvious fluorescence increase after 5 min irradiation, while **Rh-NBSe-1** shows negligible fluorescence change. Analyzing by CLSM, **Rh-NBSe** showed 3.6-fold fluorescence increase (Fig. 3b) after irradiation; however, only a slight fluorescence increase (1.1-fold) was obtained for **Rh-NBSe-1** (Fig. 3c), suggesting the photo-active ability of **Rh-NBSe** in cells. To better show the fluorescence variations of **Rh-NBSe** in real time, fluorescence imaging with different irradiation times was also recorded. As shown in Fig. 3d, the fluorescence imaging exhibits a continuous increase during 10 min, and keeps a rapid increase during 3 min (Fig. S7†). The results demonstrate a real-
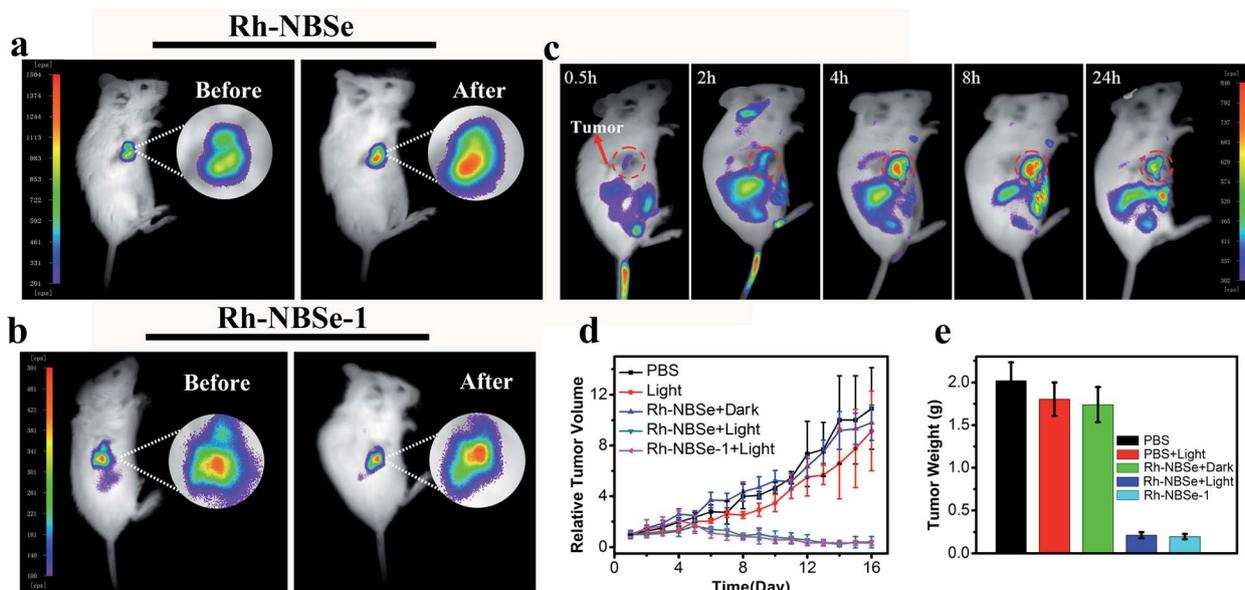

Fig. 4 The self-reporting imaging of (a) **Rh-NBSe** and (b) **Rh-NBSe-1** in mice by intratumoral injection (100 μL × 0.5 μM), before and after 5 min irradiation (660 nm, 50 mW cm^{-2}). (c) The targeted imaging of **Rh-NBSe** by intravenous injection (100 μL × 0.5 μM). (d) Relative tumor volume record. Groups: PBS, PBS + light (50 mW cm^{-2}, 8 min), **Rh-NBSe** + dark, **Rh-NBSe** + light, **Rh-NBSe-1** + light. (e) The end tumor weight of different groups. Data are shown as mean ± SD ($n = 5$).

time feedback following the irradiation time, which has potential to regulate the PDT progress.

To better study self-reporting performance *in vivo*, we also detected the fluorescence changes in BALB/c mice of subcutaneous 4T1 tumor models. For direct observation in tumors, the mice were peritumorally injected with **Rh-NBSe** or **Rh-NBSe-1**, and then the fluorescence images before/after irradiation were compared. As shown in Fig. 4a, the mice treated with **Rh-NBSe** show a ~2-fold fluorescence increase upon irradiation, identifying the photo-active ability in mice. In contrast, **Rh-NBSe-1** shows a slight fluorescence change in Fig. 4b. The results further reveal the light-dependent fluorescence increase potency of **Rh-NBSe** *in vivo*.

Imaging and therapy in mice

To verify the SIT ability of **Rh-NBSe** *in vivo*, mice were imaged after tail vein injection of **Rh-NBSe**. Though the fluorescence of **Rh** was restricted, it can still realize tumor imaging after amplification of fluorescence. As shown in Fig. 4c, **Rh-NBSe** showed obvious accumulation at the tumor site, especially after 4 h post-injection. Also the tissues and tumor imaging offered evidence for the ideal tumor targeting capability of **Rh-NBSe** (Fig. S8†). The therapeutic efficacy of **Rh-NBSe** was evaluated when the tumor volume reached 100 mm^3. Both PBS and PSs were injected intravenously. As control, tumors treated only with PBS showed a rapid increase of ~10-fold at the end, and ~9-fold increase was also observed when treated with 660 nm LED light (50 mW cm^{-2}, 8 min) or the group of **Rh-NBSe** + dark (Fig. 4d), excluding the cytotoxicity of red light or PS in dark. In comparison, tumors treated with **Rh-NBSe** and irradiation showed significant tumor growth inhibition, as the tumor volume shrank by ~0.3-fold. Similar to **Rh-NBSe**, we also evaluated the phototherapeutic ability of **Rh-NBSe-1**, for which ~0.25-fold decrease of tumor volume was obtained during 16 days, suggesting the satisfactory suppression of tumors. The final average tumor weight of the 5 groups and corresponding tumor stereogram are depicted in Fig. 4e, and the tumors are shown in Fig. S9.† The histological analysis of tumors stained by H&E also identified apoptosis and necrosis in PDT (Fig. S10†). Also, histological analysis of major organs (heart, liver, spleen, lung and kidney) (Fig. S11†) and stable mice weight changes during treatment (Fig. S12†) showed the nontoxicity of our molecules.

Conclusions

In summary, we have developed a FRET-based $^1O_2$ self-reporting PS, namely **Rh-NBSe**, which can simultaneously realize therapy, imaging and real-time therapeutic feedback. Using (*Z*)-1,2-bis(alkylthio)ethene as active linker, the **Rh-NBSe** dyad can be cleaved by $^1O_2$, restoring the fluorescence of **Rh** as feedback. The therapeutic ability has been identified in the results reported, which show satisfactory $^1O_2$ generation ($\Phi_\Delta = 0.8$) and low half maximal inhibitory concentration (IC$_{50}$ = 0.2 μM) with 5 min irradiation (20 mW cm^{-2}). Also, a 5.3-fold fluorescence recovery in PBS and 3.6-fold in cells reveal the feasible reporting

ability of **Rh-NBSe**. Moreover, the therapy and self-reporting ability were also verified in mice. Therefore, **Rh-NBSe** can realize efficient phototherapy and $^1O_2$ self-reporting ability *in vitro* and *in vivo*, and we believe that the FRET-based self-reporting PS can have potential for theranostics and monitoring.

Ethical statement

All animal operations were in accordance with institutional animal use and care regulations approved by the Model Animal Research Center of Dalian Medical University.

Conflicts of interest

There are no conflicts to declare.

Acknowledgements

Notes and references

1 F. Bray, J. Ferlay, I. Soerjomataram, R. L. Siegel, L. A. Torre and A. C. A. Jemal, *Cancer J. Clin.*, 2018, **68**, 394–424.
2 C. G. Lam, S. C. Howard, E. Bouffet and K. P. Jones, *Science*, 2019, **363**, 1182–1186.
3 W. Fan, P. Huang and X. Chen, *Chem. Soc. Rev.*, 2016, **45**, 6488–6519.
4 H. M. Kim and B. R. Cho, *Chem. Rev.*, 2015, **115**, 5014–5055.
5 A. P. Thomas, L. Palanikumar, M. T. Jeena, K. Kim and J. Ryu, *Chem. Sci.*, 2017, **8**, 8351–8356.
6 V. A. Ivanova, E. V. Verenikina, V. P. Nikitina, O. E. Zhenilo, P. A. Kruze, I. S. Nikitin and O. I. Kit, *J. Clin. Oncol.*, 2020, **38**, 6035.
7 J. Yoon, *Coord. Chem. Rev.*, 2020, **415**, 213297.
8 M. A. Rajora, J. W. H. Lou and G. Zheng, *Chem. Soc. Rev.*, 2017, **46**, 6433–6469.
9 B. M. Luby, C. D. Walsh and G. Zheng, *Angew. Chem., Int. Ed.*, 2019, **58**, 2558–2569.
10 P. C. A. Swamy, G. Sivaraman, R. N. Priyanka, S. O. Raga, K. Ponnuvel, J. Shanmugpriya and A. Gulyani, *Coord. Chem. Rev.*, 2020, **411**, 213233.
11 T. Zhang, Y. Li, Z. Zheng, R. Ye, Y. Zhang, R. T. K. Kwok, J. W. Y. Lam and B. Z. Tang, *J. Am. Chem. Soc.*, 2019, **141**, 5612–5616.
12 N. A. Pace, B. K. Rugg, C. H. Chang, O. G. Reid, K. J. Thorley, S. Parkin, J. E. Anthony and J. C. Johnson, *Chem. Sci.*, 2020, **11**, 7226–7238.
13 J. W. Foley, X. Song, T. N. Denidova, F. Jilal and M. R. Hamblin, *J. Med. Chem.*, 2006, **49**, 5291–5299.

14 K. H. Gebremedhin, M. Li, F. Gao, B. Gurram, J. Fan, J. Wang, Y. Li and X. Peng, *Dyes Pigm.*, 2019, **170**, 107617.

15 P. Wang, F. Zhou, K. Guan, X. Zhang and W. Tan, *Chem. Sci.*, 2020, **11**, 1299–1306.

16 M. Bio, G. Nkepang and Y. You, *Chem. Commun.*, 2012, **48**, 6517–6519.

17 S. Erbas-Cakmak and E. U. Akkaya, *Org. Lett.*, 2014, **16**, 2946–2949.

18 X. Meng, Y. Yang, L. Zhou, L. Zhang, Y. Lv, S. Li, Y. Wu, M. Zheng, W. Li, G. Gao, G. Deng, T. Jiang, D. Ni, P. Gong and L. Cai, *Theranostics*, 2017, **7**, 1781–1794.

19 P. Thapa, M. Li, M. Bio, P. Rajaputra, G. Nkepang, Y. Sun, S. Woo and Y. You, *J. Med. Chem.*, 2016, **59**, 3204–3214.

20 T. Xiong, M. Li, X. Zhao, Y. Zou, J. Du, J. Fan and X. Peng, *Sens. Actuators, B*, 2020, **304**, 127310–127320.

21 D. v. Straten, V. Mashayekhi, H. S. de Bruijn, S. Oliveira and D. J. Robinson, *Cancers*, 2017, **9**, 19–72.

22 M. Li, S. Long, Y. Kang, L. Guo, J. Wang, J. Fan, J. Du and X. Peng, *J. Am. Chem. Soc.*, 2018, **140**, 15820–15826.

23 G. Nkepang, M. Bio, P. Rajaputra, S. G. Awuah and Y. You, *Bioconjugate Chem.*, 2014, **25**, 2175–2188.

24 R. S. Murthy, M. Bio and Y. You, *Tetrahedron Lett.*, 2009, **50**, 1041–1044.

25 S. Erbas-Cakmak, O. A. Bozdemir, Y. Cakmak and E. U. Akkaya, *Chem. Sci.*, 2013, **4**, 858–862.

26 J. Ong, C. Lim, H. Le and W. Ang, *Angew. Chem., Int. Ed.*, 2019, **58**, 164–167.

27 Y. Yuan, C. J. Zhang, S. Xu and B. Liu, *Chem. Sci.*, 2016, **7**, 1862–1866.

28 G. Nkepang, M. Bio, P. Rajaputra, S. G. Awuah and Y. You, *Bioconjugate Chem.*, 2014, **25**, 2175–2188.

29 M. Bio, P. Rajaputra, G. Nkepang, S. G. Awuah, A. M. L. Hossion and Y. You, *J. Med. Chem.*, 2013, **56**, 3936–3942.

30 M. Bio, G. Nkepang and Y. You, *Chem. Commun.*, 2012, **48**, 6517–6519.

31 Y. Yang, S. Ko, I. Shin and J. Tae, *Nat. Protoc.*, 2007, **2**, 1740–1745.

32 Z. Yang, M. She, S. Ma, B. Yin, B. Liu, B. Liu, S. Zhao and J. Li, *Sens. Actuators, B*, 2016, **242**, 872–879.

33 M. Li, T. Xiong, J. Du, R. Tian, M. Xiao, L. Guo, S. Long, J. Fan, W. Sun, K. Shao, X. Song, J. W. Foley and X. Peng, *J. Am. Chem. Soc.*, 2019, **141**, 2695–2702.

34 E. A. Owens, S. Lee, J. Choi, M. Henary and H. S. Choi, *Wiley Interdiscip. Rev.: Nanomed. Nanobiotechnol.*, 2015, **7**, 828–838.

35 M. Li and X. Peng, *Acta Chim. Sin.*, 2016, **74**, 959–968.

36 M. Li, Y. Shao, J. H. Kim, Z. J. Pu, X. Zhao, H. Huang, T. Xiong, Y. Kang, G. Li, K. Shao, J. Fan, J. W. Foley, J. S. Kim and X. Peng, *J. Am. Chem. Soc.*, 2020, **142**, 5380–5388.

37 Z. Li, J. Wang, J. Chen, W. Lei, X. Wang and B. Zhang, *Sci. China: Chem.*, 2010, **53**, 1994–1999.

38 W. Liu, T. Liu, M. Zou, W. Yu, C. Li, Z. He, M. Zhang, M. Liu, Z. Li, J. Feng and X. Zhang, *Adv. Mater.*, 2018, **30**, e1802006.

39 W. Ou, J. H. Byeon, R. K. Thapa, S. K. Ku, C. S. Yong and J. O. Kim, *ACS Nano*, 2018, **12**, 10061–10074.